Title: Shear wave elastography can assess the in-vivo nonlinear mechanical behavior of heel-pad

Authors: Panagiotis E. Chatzistergos(*), Sara Behforootan, David Allan, Roozbeh Naemi and Nachiappan Chockalingam

(1) Staffordshire University, School of Life Science and Education, Stoke-on-Trent, UK

(*) Corresponding author: Panagiotis Chatzistergos
Panagiotis.chatzistergos@staffs.ac.uk
Leek road, Stoke-on-Trent, ST4 2 DF, UK

Abstract:

This study combines non-invasive mechanical testing with finite element (FE) modelling to assess for the first time the reliability of shear wave (SW) elastography for the quantitative assessment of the in-vivo nonlinear mechanical behavior of heel-pad. The heel-pads of five volunteers were compressed using a custom-made ultrasound indentation device. Tissue deformation was assessed from B-mode ultrasound and force was measured using a load cell to calculate the indentation test's force – deformation graph. These results were used to design subject specific FE models and to inverse engineer the tissue's hyperelastic material coefficients and its stress - strain behavior. SW speed was measured for different levels of compression (from 0% to 50% compression). SW speed for 0% compression was used to assess the initial stiffness of heel-pad (i.e. initial shear modulus, initial Young's modulus). Changes in SW speed with increasing compressive loading were used to quantify the tissue's nonlinear mechanical behavior based on the theory of acoustoelasticity. Statistical analysis of results showed significant correlation between SW-based and FE-based estimations of initial stiffness, but SW underestimated initial shear modulus by 64%(±16). A linear relationship was found between the SW-based and FE-based estimations of nonlinear behavior. The results of this study indicate that SW elastography is capable of reliably assessing differences in stiffness, but the absolute values of stiffness should be used with caution. Measuring changes in SW speed for different magnitudes of compression enables the quantification of the tissue's nonlinear behavior which can significantly enhance the diagnostic value of SW elastography.

Keywords: soft tissue, acoustoelasticity, validation, ultrasound, mechanical testing, finite element

1. Introduction

Heel-pad is a highly specialized tissue with nonlinear, visco-elastic mechanical behavior and complex internal structure. It comprises fat globules enclosed within a matrix of fibrous connective tissue (Campanelli et al., 2011) and its primary role is to act as a shock absorber that dampens the effect of impact forces during locomotion and promotes a more even distribution of plantar loading. The internal structure and mechanical properties of heel-pad is affected by aging (Kwan R.LC., Zheng YP. et al., 2010), injury and disease (Pai and Ledoux, 2012, 2010; Rome et al., 2001) which in turn can make it more vulnerable to trauma (Sara Behforootan et al., 2017b). Being able to reliably assess the mechanical characteristics of heel-pad in the clinic can enhance the clinical management of conditions such as diabetic foot, heel pain syndrome, etc. (C. Y. Lin et al., 2017; Naemi et al., 2017).

Shear wave (SW) elastography is a non-invasive, ultrasound-based method for the quantitative assessment of the stiffness of soft tissues. It involves the generation of SWs inside the imaged tissue and the measurement of their propagation speed as they expand laterally in the field of view. Measurements of SW speed can be used to detect regional differences in the mechanical properties of tissues and to estimate the tissue's shear modulus (G) and Young's modulus (E) based on the following formula:

$$E = 3G = 3\rho C^2, \quad (1)$$

Where C is the SW propagation speed and ρ is the tissue's density ($\rho \approx 1000$ kg/m^3 for soft tissues).

The relationship between SW speed and Young's modulus of equation 1, is based on the assumption that the imaged material is incompressible, homogeneous, isotropic and linearly elastic (Bercoff et al., 2004; Widman et al., 2015). Even though these assumptions might seem to be restrictive, SW elastography has been successfully integrated into clinical practice for the diagnosis of conditions that are strongly associated with altered tissue stiffness such as chronic liver disease or breast cancer etc. (Sigrist et al., 2017). However, the fact that no biological tissue fully complies with the aforementioned

conditions means that careful validation of SW results in individual tissues is a key prerequisite for any clinical use.

SW elastography has already been used to investigate the biomechanics of heel-pad and has provided new insight on the heterogeneity of its mechanical characteristics (Lin et al., 2015; C. Lin et al., 2017; C. Y. Lin et al., 2017; Wu et al., 2017) and its possible clinical uses (Lin et al., 2015; C. Lin et al., 2017). In one of the first studies to use SW elastography in the heel-pad, Lin et al. (2015) established that SW is a repeatable measurement. However, the validity of the predicted values of shear modulus or Young's modulus has not been assessed yet.

Validation of the estimations of SW elastography requires a prior knowledge of the tissue's mechanical properties. This makes validation a very challenging task and for this reason validation studies have been limited to the use of phantoms (Carlsen et al., 2015; Chatelin et al., 2014; Widman et al., 2015) or ex-vivo samples (Aristizabal et al., 2017; Eby et al., 2013). The ability of SW to accurately predict the in-vivo nonlinear mechanical behavior of soft tissues has not been tested yet.

The combined use of in-vivo testing and computer modelling is the only method for the non-invasive calculation of the material properties of soft tissues. In the case of heel-pad, ultrasound indentation and finite element (FE) modelling were successfully combined in previous studies for the assessment of its material properties and the calculation of its in-vivo stress–strain behavior (Behforootan et al., 2017; Chatzistergos et al., 2015; Erdemir et al., 2006).

Given that SW speed is affected by the internal stress-state of the imaged tissue (Ateş et al., 2018; Syversveen et al., 2012), the guidelines for the clinical use of SW elastography indicate that the minimum possible compression should be applied to the tissue during imaging (Cosgrove et al., 2013). However, imaging the tissue in an unloaded state provides an assessment of stiffness for very low strains

only and cannot provide any information on its nonlinear response to loading (Aristizabal et al., 2017; Bernal et al., 2016; Latorre-Ossa et al., 2012). Being able to assess the nonlinear mechanical behavior of soft tissues would significantly enhance the diagnostic potential of elastography (Aristizabal et al., 2017; Bernal et al., 2016; Latorre-Ossa et al., 2012).

Acoustoelasticity theory explains the changes in SW propagation speed inside an elastic and quasi-incompressible material under static compression based on the following formula:

$$\rho C^2 = G_0^{SW} - \sigma \frac{A}{12 G_0^{SW}}, \quad (2)$$

where G_0 is the tissue's shear modulus for zero compression (i.e. initial shear modulus), σ is the compressive stress inside the tissue and A is the tissue's nonlinear shear modulus. Considering equation 1, equation 2 can be rewritten to estimate the instantaneous shear modulus (G_i^{SW}) based on the compressive stress of each loading step:

$$G_i^{sw} = G_0^{sw} - \sigma_i \frac{A}{12 G_0^{sw}}, \quad (3)$$

The potential of acoustoelasticity to provide an assessment of the nonlinear mechanical behavior of soft tissues has been demonstrated in tests involving phantom samples (Bernal et al., 2016; Latorre-Ossa et al., 2012) or ex-vivo kidney samples (Aristizabal et al., 2017).

In this context, the aim of this study was to combine non-invasive mechanical testing with FE modelling to assess the reliability of SW elastography for the assessment of the in-vivo biomechanics of heel-pad.

The feasibility of using SW elastography to quantify the nonlinear mechanical behavior of plantar soft tissue was also assessed.

2. Methods

2.1 In-vivo testing

Five healthy volunteers with average(±stdev) age, weight and height of 32(±6) y, 73(±12) kg and 168(±9) cm respectively were recruited for this study. The left foot of each participant was subjected to stepwise indentation to study the nonlinear, elastic mechanical response of heel-pad to compression.

Mechanical testing was performed using a custom-made ultrasound indentation device that enables controlled and repeatable loading of the soft tissues of the sole of the foot (Behforootan et al., 2017; Chatzistergos et al., 2015). After fixing the participant's foot on the device, their heel was covered with coupling gel and the ultrasound probe was positioned perpendicular to the plantar surface to image the apex of the calcaneus in the sagittal plane. A linear array ultrasound probe (4-15 MHz, SL 15-4 Linear transducer, SuperSonic Imagine Ltd), which is acting also as the indenter, was moved slowly towards the foot and the initial thickness of the heel-pad was measured from the first ultrasound image where the calcaneus was visible. The indenter was moved using a motor which could be programmed to realize a predefined loading protocol (Sara Behforootan et al., 2017b).

During testing, compressive force was recorded at 100 Hz using a load cell (Zemic load cell, L6E, C3) which was in series with the ultrasound probe. B-mode ultrasound images and SW elastography images (elastograms) were recorded at 11Hz by the ultrasound unit (Aixplorer®, SuperSonic Imagine, Aix-en-Provence, France). A stand-off (Sonokit, Sonogel, Vertriebs, Gmbh, Sonic velocity 1405 m/s,

absorption 0.09 dB/MHz.mm and reflection: 2.4%) was used to improve docking between transducer and skin.

Every test was preceded by seven preconditioning loading/ unloading cycles to maximum compression at 0.5 mm/ s to minimize the effect of loading history (Behforootan et al., 2017). After preconditioning, heel-pad was compressed in five steps to a maximum of 50% of its original thickness. At each step, a displacement equal to 10% of heel-pad's thickness was imposed at a comfortable speed (0.5 mm/ s) and then kept constant for 60 s before the next loading step was imposed. Measurements of force, deformation and SW speed were extracted only for the last second of each relaxation period. The duration of the relaxation period was decided based on previous work on the stress – relaxation behavior of heel-pad (Behforootan et al., 2017). A series of preliminary tests were performed on each participant to verify that 60 s of relaxation time was sufficient to minimize the effect of viscosity on results. More details on these preliminary tests are presented in Supplementary material.

Preliminary testing indicated that the elastograms of heel-pad can be separated into two layers with relatively uniform and distinctively different SW speeds (figure 1): a more superficial, stiffer layer (layer-1) and a deeper, softer one (layer-2). It is reported in literature that good quality elastograms can be consistently recorded only for the most superficial ≈10mm of the heel-pad (C. Y. Lin et al., 2017). This observation was also verified during the preliminary tests of this study and led to limiting the measurement of SW speed to layer-1 only. More specifically SW speed was measured within a circular area defined by the boundaries of layer-1 and aligned with the apex of the curvature of the calcaneus (Figure 1).

To measure the deformation of layer 1, the interface between the two layers was identified with the help of SW elastograms for the unloaded heel and then, as the heel was loaded, changes in the thickness of layer-1 were assessed in B-mode images. The measurements of deformation were combined with

measurements of force to calculate one force–deformation graph for layer-1 and one for the entire heel-pad.

The measured SW speed was used to estimate heel-pad's shear modulus and Young's modulus for the case of the unloaded heel (G_0^{SW}, E_0^{SW}) and for each loading step (G_i^{SW}, E_i^{SW}: $1 \leq i \leq 5$) using equation 1. The variations of SW speed between different loading steps was used to assess heel-pad's nonlinear shear modulus (A) based on equation 3. For this purpose, the compressive stress of each loading step (σ_i) was estimated from Hooke's law using the definition for cumulative stress in incompressible materials (Aristizabal et al., 2017; Gennisson et al., 2007; Latorre-Ossa et al., 2012):

$$\sigma_i = \sum_{j=1}^{i} \Delta\sigma_j = \sum_{j=1}^{i} 3G_j\Delta\varepsilon_j, \quad (4)$$

where $\Delta\varepsilon_j$ is the differential strain of each loading step. Shear modulus (G_i^{SW}) was plotted over cumulative stress (σ_i) for each loading step and a straight line with fixed intercept, equal to G_0^{SW}, was fitted to the data. According to equation 3, the slope of this straight line was then used to calculate the nonlinear shear modulus (A).

2.2 FE modelling

A previously validated computational technique for subject-specific FE modeling and the inverse engineering of heel-pad's material coefficients was used (Behforootan et al., 2017). In its original form this technique utilized sagittal and frontal ultrasound images of the heel to reconstruct the 3D geometry of heel-pad assuming that heel-pad consists of a single hyperelastic material. The produced subject-specific FE models were then used to simulate the indentation test and estimate its force-deformation graph. The indentation tests were simulated by fixing the areas of the calcaneus and imposing a displacement to the model of the probe. Frictionless contact was assumed between the probe and the

heel. The values of the material coefficients of bulk heel-pad that minimized the difference between the numerically estimated and the in-vivo measured force-deformation graph were calculated using an optimization-based iterative process (Behforootan et al., 2017).

For the purpose of this study, the aforementioned technique was modified to include two layers of materials with different thickness and material coefficients instead of one (Figure 2). The mechanical behavior of the two layers of heel-pad was simulated using the Ogden hyperelastic (1st order) material model:

$$W = \frac{\mu}{\alpha}\left(\overline{\lambda}_1^{\,\alpha} + \overline{\lambda}_2^{\,\alpha} + \overline{\lambda}_3^{\,\alpha} - 3\right) + \frac{1}{d}(J-1)^2, \quad (5)$$

where $\overline{\lambda}_p^{\,a}(p = 1,2,3)$ are the deviatoric principal stretches, J is the determinant of elastic deformation gradient and μ, α and d are material coefficients. Coefficient α is related to the tissue's nonlinear stress – strain behaviour while μ and α can be used to estimate its initial shear modulus (G_0^{FE}):

$$G_o^{FE} = \frac{1}{2}\mu\alpha, \quad (6)$$

Coefficient d is directly related to Poisson's ratio (ν), therefore assuming that heel-pad is nearly incompressible (ν=0.475) leaves only material coefficients μ, α that need to be inverse engineered. More specifically the material coefficients of both layers were inverse engineered to minimise the difference between the numerical and the in-vivo force-deformation graphs for the entire heel-pad and for layer-1 at the same time. All FE simulations were performed using ANSYS 16.0 (ANSYS, Canonsburg, PA, USA).

The subject-specific material coefficients for layer-1 were used to calculate the tissue's compressive stress-strain behaviour and assess its initial slope (E_0^{FE}) and its slope for the strain of each load step (E_i^{FE}: $1 \leq i \leq 5$).

2.3 Comparison between SW and FE

The difference between the values of initial shear modulus that were calculated from SW speed using equation 1 and those that were calculated from the subject-specific material coefficients using equation 6 was assessed. The relationship between the SW-based nonlinear shear modulus (A) and FE-based material coefficient α was investigated. These two output measures were analysed together because both of them quantify the nonlinear nature of a tissue's mechanical behaviour.

The method of generalized estimating equations (GEE) was used to investigate the relationship between SW-based calculations of Young's modulus and the FE-based ones for all load steps (Eby et al., 2013). GEE is an extension of the generalized linear model that accounts for repeated measurements and therefore it enables combining, in the same analysis, the repeated measures for different loading steps for all participants. The goodness-of-fit of the linear model was assessed by calculating the coefficient of determination (R^2)(Eby et al., 2013). GEE analysis was performed using IBM® SPSS®v.21.

3. Results

3.1 In-vivo testing

The average(±stdev) heel-pad thickness was 19.7(±3.4) mm and 41%(±3%) of the total thickness was identified as layer-1 (Table 1). The maximum strain for layer-1was, on average, equal to the 46%(±19%) of the strain of layer-2 verifying that layer-1 is stiffer than the rest of the heel-pad.

The average value of initial shear modulus (G_0^{SW}) was 56(±21) kPa and consistently increased with compression (Table 2). Figure 3 presents the values of shear modulus for each loading step over compressive stress for each of the participants. As it can be seen, their relationship for each participant can be defined using a straight line with a fixed intercept in accordance with equation 3 of acoustoelastic theory ($0.84 \leq R^2 \leq 0.93$). The slope of the aforementioned lines was used to calculate the nonlinear shear modulus (A) for each participant (table 2). The average value of A was -940 kPa (±381 kPa). Considering equation 3, the negative value A indicates that shear modulus increases with loading; a behaviour that is consistent with a hyperelastic material.

3.2 FE modelling

The average values of the material coefficients μ and α and of the initial shear modulus of layer-1 was 15.5 (±6.3) kPa, 22.2 (±5.7) and 179 (±104) kPa respectively (table 3). Layer-2 was substantially softer than layer-1. The average difference between the two layers in terms of initial shear modulus was 78%(±16%).

3.3 Comparison between FE and SW

Comparison between the results for initial shear modulus from SW elastography and FE modelling indicated a substantial and systematic underestimation by SW. On average the difference between the two methods was 64%(±16%).

GEE analysis of measurements for all load steps and all participants revealed a significant correlation between the SW-based calculation of Young's modulus and the FE-based ones ($p=0.002$). The regression coefficient was 3.74 with a 95% confidence interval of 1.43-6.04. The goodness-of-fit of the produced linear relationship was $R^2= 0.59$ (figure 4).

Plotting SW-based results over FE-based ones for all participants revealed a linear relationship between the non-linear shear modulus (A) and material coefficient α, namely between the SW-based and FE-based measures respectively of nonlinear behavior (Figure 5). As it can be seen in figure 5, the absolute value of the SW-based measure of nonlinearity (A) increases with the FE-based one (α) showing a high coefficient of determination ($R^2 = 0.91$). In both cases higher absolute values indicate a more nonlinear mechanical behaviour.

4. Discussion

For the first time, the validity of material properties from SW is directly assessed against relevant measurements that reflect the in-vivo mechanical behaviour of heel-pad. The results indicate a significant linear relationship between SW-based and FE-based estimations of initial stiffness.

The combined use of in-vivo testing and FE modelling enabled the calculation of subject-specific material coefficients and of the actual stress–strain graphs of heel-pad. For this purpose, a previously validated method for subject-specific modelling and inverse engineering was modified and utilised (Behforootan et al., 2017). This enabled the calculation of initial shear modulus and initial Young's modulus as well as of the instantaneous Young's modulus for strains equal to the ones imposed during each loading step.

Comparison between SW-based and FE-based estimations of initial stiffness of the tissue revealed a systematic underestimation of initial shear modulus by SW, however a significant linear relationship between the two was observed. These findings indicate that SW elastography is capable of reliably identifying tissues with different stiffness. However, the absolute values of the predicted mechanical properties should be used with caution.

Going beyond the conventional use of SW elastography, the variation of SW-based measurements of shear modulus under different magnitudes of compression was used to quantify heel-pad's nonlinear mechanical behavior. According to the theory of acoustoelasticity, the SW-predicted shear modulus inside an elastic and quasi-incompressible body changes linearly with the magnitude of static compressive stress (equation 3). This hypothesis was validated for the heel-pad by the results of this study (figure 3) which opened the way for the calculation of its in-vivo nonlinear shear modulus (A). Previous studies calculated nonlinear shear modulus only for phantom materials (Gennisson et al., 2007; Latorre-Ossa et al., 2012) or for ex-vivo tissue samples (Aristizabal et al., 2017).

A comparison between A and the value of material coefficient α, which is the FE-based measure of nonlinear mechanical behavior, revealed a linear relationship between the two (figure 5). This relationship indicates that SW elastography is capable of quantifying the nonlinear nature of the mechanical behavior of soft tissues and it can differentiate between tissues that exhibit a less strong nonlinear behavior from tissues with stronger nonlinear behavior. This unique ability can enhance the diagnostic capacity of SW elastography (Aristizabal et al., 2017; Gennisson et al., 2007; Latorre-Ossa et al., 2012).

For the purpose of this study, non-invasive testing was performed using a custom-made indentation device which compressed the heel-pad in individual steps with a wait period between them (i.e. stepwise compression). Stepwise compression was used instead of continuous loading, because elastograms need a few seconds to stabilise after movement which makes the reliable measurement of SW speed during continous loading very challenging (Aristizabal et al., 2017; Wu et al., 2017). At the same time, step-wise compression also reduces the risk of injury by avoiding the prolonged application of concentrated loading of quasi-static testing. In a previous study where stepwise compression was used with SW elastography it was found that the results were influenced by the viscoelastic nature of the imaged tissue (Aristizabal et al., 2017). In the present study a relaxation period of 60 s between loading steps was found to be needed to minimise the effect of viscocity on the results (Suplimentary material).

The internal structure of the fat-pad comprises a more superficial layer of fatty microchambers, which is relatively thin and stiff, and a deeper layer of macrochambers, which is relatively thick and soft (Hsu et al., 2007; Kelikian and Sarrafian, 2011). These two parts of the heel are divided by a thin fibrous layer (Kelikian and Sarrafian, 2011). In the present study heel-pad was divided into two layers, but these layers do not correspond to the aforementioned anatomical layers of microchambers or macrochambers. This is because preliminary testing indicated that the boundary between

348 microchambers and macrochambers could not be reliably tracked between loading steps. To overcome
349 this difficulty and to enhance the reliability of the measurement of strain, two layers with relative
350 uniform SW speed were defined based on the SW elastograms (figure 1). The boundary between these
351 two layers could be identified easily in the images of the unloaded heel and could be reliably tracked
352 between loading steps.

353

354 Like microchambers and macrochambers, in this case the more superficial layer (layer-1) was thinner
355 and stiffer than the deeper one (layer-2). The measured initial shear modulus for layer-1 was 56 kPa
356 (±21 kPa) which is very similar to relevant measurements from literature for microchamber layer (Wu
357 et al., 2017). A previous SW-based investigation of the mechanical properties of the two anatomical
358 layers in young healthy individuals indicated that the initial shear modulus of microchambers is 60.1
359 kPa (±9.8 kPa) and the initial shear modulus of macrochambers is 27.7 kPa (±4.9 kPa) (Wu et al., 2017).
360 Layer-1 was thicker than the reported thickness of microchambers in literature (Hsu et al., 2007). More
361 specifically, the thickness of layer-1 was around 70% of the thickness for layer-2. According to
362 literature the thickness of the microchamber layer is around 30% of the thickness of the macrochamber
363 layer (Hsu et al., 2007). Based on these, it can be concluded that the definition of layers in this study
364 was not aligned with the anatomical layers of heel-pad, but the results for layer-1 appear to be relevant
365 to the microchambers layer.

366

367 This apparent discrepancy between the definition of layers from B-mode or SW images can also be
368 observed in previously published results of SW elastography of the heel-pad (Wu et al., 2017). More
369 specifically in the ultrasound images presented by Wu et al., 2017, the area of relatively stiff tissue
370 appears to penetrate the area defined as macrochambers. A possible explanation for these observations
371 is that the superficial stiff layer defined from SW elastography (layer-1) expands beyond the
372 microchamber layer and into the transitional fibrous tissue that separates the two layers of adipose
373 tissue.

In this study the predictions of SW elastography about the mechanical properties of heel-pad were compared against relevant FE-based measurements using a previously validated technique (Sara Behforootan et al., 2017a). Even though FE modelling has its own limitations and it could not be considered as a "gold standard" method, it is the only method for the non-invasive assessment of in-vivo mechanical properties of tissues (Akrami et al., 2018; Sara Behforootan et al., 2017a). In the case of this study the reliability of FE-based calculations is significantly enhanced by the combined use of in-vivo testing and FE modelling.

Moreover, because of the relatively small number of participants, drawing generalizable conclusions about heel-pad biomechanics from the results of this study is very difficult. At the same time, the comparison between SW-based and FE-based predictions presented here can give new insight on the validity and clinical relevance of the results of SW elastography.

The proposed method is significantly easier to be implemented in a clinic compared to existing methods for the assessment of the nonlinear mechanical behavior of plantar soft tissue and could significantly enhance research and clinical practice (Sara Behforootan et al., 2017a; Erdemir et al., 2006; Williams et al., 2017). Particularly in the area of computer modelling the proposed method can support the use of subject-specific material properties which would significantly improve the reliability and clinical relevance of FE models of the foot (Akrami et al., 2018). Moreover, previous research has highlighted the potential value of measuring plantar soft tissue biomechanics in the clinic for the management of conditions such as diabetic foot (Akrami et al., 2018; Naemi et al., 2017). With regards to clinical use, the main disadvantage of this method against previous ultrasound-based techniques (Sara Behforootan et al., 2017a; Erdemir et al., 2006) is the cost of SW elastography which remains relatively high compared to conventional ultrasound.

The results of this study indicate that SW elastography can be used to quantify differences in the initial shear modulus and Young's modulus of heel-pad as well as in its nonlinear mechanical behavior. The methods presented here can influence the protocols and procedures for the clinical use of SW elastography in foot-related applications and beyond with a view to increase diagnostic accuracy.

5. Conflict of interest: None

6. Acknowledgments:

Technical support from SuperSonic Imagine Ltd. is kindly acknowledged.

423 **References**

424 Akrami, M., Qian, Z., Zou, Z., Howard, D., Nester, C.J., Ren, L., 2018. Subject-specific finite element
425 modelling of the human foot complex during walking: sensitivity analysis of material properties,
426 boundary and loading conditions. Biomech. Model. Mechanobiol. 17, 559–576.
427 https://doi.org/10.1007/s10237-017-0978-3

428 Aristizabal, S., Amador, C., Nenadic, I.Z., Greenleaf, J.F., Urban, M.W., 2017. Application of
429 Acoustoelasticity to Evaluate Nonlinear Modulus in ex vivo Kidneys. IEEE Trans. Ultrason.
430 Ferroelectr. Freq. Control 65, 188–200. https://doi.org/10.1109/TUFFC.2017.2781654

431 Ateş, F., Andrade, R.J., Freitas, S.R., Hug, F., Lacourpaille, L., Gross, R., Yucesoy, C.A., Nordez, A.,
432 2018. Passive stiffness of monoarticular lower leg muscles is influenced by knee joint angle.
433 Eur. J. Appl. Physiol. 0, 1–9. https://doi.org/10.1007/s00421-018-3798-y

434 Behforootan, S., Chatzistergos, P., Naemi, R., Chockalingam, N., 2017a. Finite Element Modelling of
435 the Foot for Clinical Applications: a Systematic Review. Med. Eng. Phys. 39, 1–11.
436 https://doi.org/10.1016/j.medengphy.2016.10.011

437 Behforootan, S., Chatzistergos, P.E., Chockalingam, N., Naemi, R., 2017b. A clinically applicable
438 non-invasive method to quantitatively assess the visco-hyperelastic properties of human heel
439 pad, implications for assessing the risk of mechanical trauma. J. Mech. Behav. Biomed. Mater.
440 68, 287–295. https://doi.org/10.1016/j.jmbbm.2017.02.011

441 Behforootan, S., Chatzistergos, P.E., Chockalingam, N., Naemi, R., 2017c. A Simulation of the
442 Viscoelastic Behaviour of Heel Pad During Weight-Bearing Activities of Daily Living. Ann.
443 Biomed. Eng. 45, 2750–2761. https://doi.org/10.1007/s10439-017-1918-1

444 Bercoff, J., Tanter, M., Fink, M., 2004. Supersonic shear imaging: a new technique for soft tissue
445 elasticity mapping. IEEE Trans. Ultrason. Ferroelectr. Freq. Control 51, 396–409.
446 https://doi.org/10.1109/TUFFC.2004.1295425

447 Bernal, M., Chamming's, F., Couade, M., Bercoff, J., Tanter, M., Gennisson, J.-L., 2016. In Vivo
448 Quantification of the Nonlinear Shear Modulus in Breast Lesions: Feasibility Study. IEEE

449 Trans. Ultrason. Ferroelectr. Freq. Control 63, 101–9.
450 https://doi.org/10.1109/TUFFC.2015.2503601

451 Campanelli, V., Fantini, M., Faccioli, N., Cangemi, A., Pozzo, A., Sbarbati, A., 2011. Three-
452 dimensional morphology of heel fat pad: an in vivo computed tomography study. J. Anat. 219,
453 622–631. https://doi.org/10.1111/j.1469-7580.2011.01420.x

454 Carlsen, J.F., Pedersen, M.R., Ewertsen, C., Sãftoiu, A., Lönn, L., Rafaelsen, S.R., Nielsen, M.B.,
455 2015. A comparative study of strain and shear-wave elastography in an elasticity phantom. Am.
456 J. Roentgenol. 204, W236–W242. https://doi.org/10.2214/AJR.14.13076

457 Chatelin, S., Bernal, M., Deffieux, T., Papadacci, C., Flaud, P., Nahas, A., Boccara, C., Gennisson, J.-
458 L., Tanter, M., Pernot, M., 2014. Anisotropic polyvinyl alcohol hydrogel phantom for shear
459 wave elastography in fibrous biological soft tissue: a multimodality characterization. Phys. Med.
460 Biol. 59, 6923–6940. https://doi.org/10.1088/0031-9155/59/22/6923

461 Chatzistergos, P.E., Naemi, R., Chockalingam, N., 2015. A method for subject-specific modelling and
462 optimisation of the cushioning properties of insole materials used in diabetic footwear. Med.
463 Eng. Phys. 37, 531–538. https://doi.org/10.1016/j.medengphy.2015.03.009

464 Cosgrove, D., Piscaglia, F., Bamber, J., Bojunga, J., Correas, J.-M., Gilja, O., Klauser, A., Sporea, I.,
465 Calliada, F., Cantisani, V., D'Onofrio, M., Drakonaki, E., Fink, M., Friedrich-Rust, M.,
466 Fromageau, J., Havre, R., Jenssen, C., Ohlinger, R., Săftoiu, A., Schaefer, F., Dietrich, C., 2013.
467 EFSUMB Guidelines and Recommendations on the Clinical Use of Ultrasound
468 Elastography.Part 2: Clinical Applications. Ultraschall der Medizin - Eur. J. Ultrasound 34, 238–
469 253. https://doi.org/10.1055/s-0033-1335375

470 Eby, S., Song, P., Chen, S., Chen, Q., Greenleaf, J., An, K.-N., 2013. Validation of shear wave
471 elastography in skeletal muscle. J. Biomech. 46, 2381–2387.
472 https://doi.org/10.1016/j.jbiomech.2013.07.033

473 Erdemir, A., Viveiros, M.L., Ulbrecht, J.S., Cavanagh, P.R., 2006. An inverse finite-element model of
474 heel-pad indentation. J. Biomech. 39, 1279–1286.

https://doi.org/10.1016/j.jbiomech.2005.03.007

Gennisson, J.-L., Rénier, M., Catheline, S., Barrière, C., Bercoff, J., Tanter, M., Fink, M., 2007. Acoustoelasticity in soft solids: Assessment of the nonlinear shear modulus with the acoustic radiation force. J. Acoust. Soc. Am. 122, 3211–3219. https://doi.org/10.1121/1.2793605

Hsu, C.-C., Tsai, W.-C., Wang, C.-L., Pao, S.-H., Shau, Y.-W., Chuan, Y.-S., 2007. Microchambers and macrochambers in heel pads: are they functionally different? 102. https://doi.org/10.1152/japplphysiol.01137.2006

Kelikian, A.S., Sarrafian, S.K., 2011. Functional Anatomy of the Foot and Ankle, in: Sarrafian's Anatomy of the Foot and Ankle : Descriptive, Topographical, Functional. Wolters Kluwer Health/Lippincott Williams & Wilkins, p. 633.

Kwan R.LC., Zheng YP., C.G.L., Kwan, R.L.-C., Zheng, Y.-P., Cheing, G.L.-Y., 2010. The effect of aging on the biomechanical properties of plantar soft tissues. Clin. Biomech. (Bristol, Avon) 25, 601–5. https://doi.org/10.1016/j.clinbiomech.2010.04.003

Latorre-Ossa, H., Gennisson, J.L., De Brosses, E., Tanter, M., 2012. Quantitative imaging of nonlinear shear modulus by combining static elastography and shear wave elastography. IEEE Trans. Ultrason. Ferroelectr. Freq. Control 59, 833–839. https://doi.org/10.1109/TUFFC.2012.2262

Lin, C.-Y., Lin, C.-C., Chou, Y.-C., Chen, P.-Y., Wang, C.-L., 2015. Heel Pad Stiffness in Plantar Heel Pain by Shear Wave Elastography. Ultrasound Med. Biol. 41, 2890–8. https://doi.org/10.1016/j.ultrasmedbio.2015.07.004

Lin, C., Wu, C., Özçakar, L., 2017. Restoration of Heel Pad Elasticity in Heel Pad Syndrome Evaluated by Shear Wave Elastography. Am. J. Phys. Med. &amp 96, e96. https://doi.org/10.1097/phm.0000000000000655

Lin, C.Y., Chen, P.Y., Shau, Y.W., Tai, H.C., Wang, C.L., 2017. Spatial-dependent mechanical properties of the heel pad by shear wave elastography. J. Biomech. 53, 191–195. https://doi.org/10.1016/j.jbiomech.2017.01.004

Naemi, R., Chatzistergos, P., Suresh, S., Sundar, L., Chockalingam, N., Ramachandran, A., 2017. Can plantar soft tissue mechanics enhance prognosis of diabetic foot ulcer? Diabetes Res. Clin. Pract. 126, 182–191. https://doi.org/10.1016/j.diabres.2017.02.002

Pai, S., Ledoux, W.R., 2012. The shear mechanical properties of diabetic and non-diabetic plantar soft tissue. J. Biomech. 45, 364–70. https://doi.org/10.1016/j.jbiomech.2011.10.021

Pai, S., Ledoux, W.R., 2010. The compressive mechanical properties of diabetic and non-diabetic plantar soft tissue. J. Biomech. 43, 1754–60. https://doi.org/10.1016/j.jbiomech.2010.02.021

Rome, K., Webb, P., Unsworth, A., Haslock, I., 2001. Heel pad stiffness in runners with plantar heel pain. Clin. Biomech. (Bristol, Avon) 16, 901–5.

Sigrist, R.M.S., Liau, J., Kaffas, A. El, Chammas, M.C., Willmann, J.K., 2017. Ultrasound Elastography: Review of Techniques and Clinical Applications. Theranostics 7, 1303–1329. https://doi.org/10.7150/thno.18650

Syversveen, T., Midtvedt, K., Berstad, A.E., Brabrand, K., Strøm, E.H., Abildgaard, A., 2012. Tissue elasticity estimated by acoustic radiation force impulse quantification depends on the applied transducer force: an experimental study in kidney transplant patients. Eur. Radiol. 22, 2130–7. https://doi.org/10.1007/s00330-012-2476-4

Widman, E., Maksuti, E., Larsson, D., Urban, M.W., Bjällmark, A., Larsson, M., 2015. Shear wave elastography plaque characterization with mechanical testing validation: A phantom study. Phys. Med. Biol. 60, 3151–3174. https://doi.org/10.1088/0031-9155/60/8/3151

Williams, E.D., Stebbins, M.J., Cavanagh, P.R., Haynor, D.R., Chu, B., Fassbind, M.J., Isvilanonda, V., Ledoux, W.R., 2017. A preliminary study of patient-specific mechanical properties of diabetic and healthy plantar soft tissue from gated magnetic resonance imaging. Proc. Inst. Mech. Eng. Part H J. Eng. Med. 231, 625–633. https://doi.org/10.1177/0954411917695849

Wu, C.H., Lin, C.Y., Hsiao, M.Y., Cheng, Y.H., Chen, W.S., Wang, T.G., 2017. Altered stiffness of microchamber and macrochamber layers in the aged heel pad: Shear wave ultrasound elastography evaluation. J. Formos. Med. Assoc. 4–9. https://doi.org/10.1016/j.jfma.2017.05.006

Tables:

Table 1: The measured thickness of the entire heel pad and of layer-1 when the heel is not subjected to any compression and under maximum compression.

Participants	Original thickness (mm)		Maximum deformation (mm)	
	Total	Layer-1	Total	Layer-1
#1	25.0	10.6	3.8	1.37
#2	19.3	9.0	3.8	0.80
#3	20.4	8.3	5.2	1.02
#4	16.7	6.4	5.7	1.01
#5	16.8	6.4	5.7	1.35
Average	19.7	8.1	4.9	1.11
STDEV	3.4	1.8	1.0	0.24

Table 2: The SW-predicted shear modulus (G_i) for all participants and all loading steps ($0 \leq i \leq 5$). The values of the nonlinear shear modulus (A) that is calculated based on the variation of shear modulus between loading steps is also presented.

Participant	G_0 (kPa)	G_1 (kPa)	G_2 (kPa)	G_3 (kPa)	G_4 (kPa)	G_5 (kPa)	A (kPa)
#1	88	90	104	112	132	149	-1145
#2	58	62	72	85	98	106	-1494
#3	49	50	58	66	74	88	-813
#4	53	64	71	76	83	104	-718
#5	29	72	88	106	123	139	-533
Average	56	68	79	89	102	117	-941
STDEV	21	15	18	20	25	26	381

Table 3: The values of the subject-specific material coeffcients for the two layers (μ, α). The FE based calcaultion of initial shear modulus is also presented for all participants.

Participant	Layer-1			Layer-2		
	μ (kPa)	α	G_0 (kPa)	μ (kPa)	α	G_0 (kPa)
#1	24.3	24.3	296	14.4	20.2	145
#2	19.3	30.0	290	9.2	10.0	46
#3	9.7	23.3	114	4.1	10.1	21
#4	9.7	18.0	88	2.0	13.0	13
#5	14.2	15.3	109	1.0	23.0	11
Average	15.5	22.2	179	6.1	15.3	47
STDEV	6.3	5.7	104	5.6	6.0	56

583 **Figure legends:**

584

585 Figure 1: A typical SW elastography image of the heel-pad under minimum compression. The
586 interface between the more superficial, stiffer layer-1 and the deeper, softer layer-2 is highlighted
587 using a horizontal dotted line. This interface was used to define the cyclic area where SW speed was
588 assessed and to measure the deformation of layer-1.

589

590 Figure 2: The FE model of the indentation test under no compression (top) and under maximum
591 compression (down).

592

593 Figure 3: The variation of SW-based measurements of shear modulus (G^{SW}) with compressive stress
594 (σ) for all participants. Straight lines with fixed intercepts were fitted to the data in accordance to
595 equation 3. The value of R^2 that quantifies goodness-of-fit of the linear relationships is also presented
596 for each participant.

597

598 Figure 4: Scatter-plot of the FE-based calculations of Young's modulus (E^{FE}) over the SW-based ones
599 (E^{SW}) for all loading steps and for all participants. The linear relationship that was calculated from
600 GEE is also presented along with the value of R^2 for goodness-of-fit.

601

602 Figure 5: The relationship between the SW-based and the FE-based parameters that quantify the
603 nonlinearity of the mechanical behavior of heel-pad, namely between the nonlinear shear modulus (A)
604 and the unitless material coefficient (α) of the Ogden model.

605

606

607

608

609

610

Figures:

Figure 1

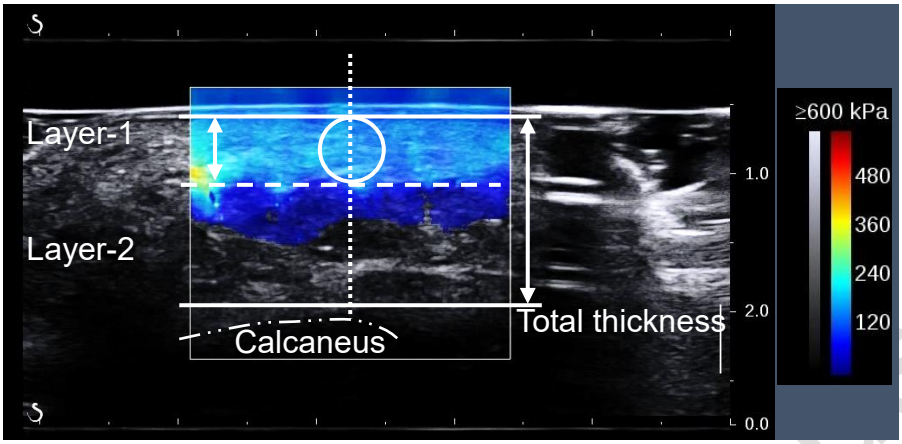

Figure 2

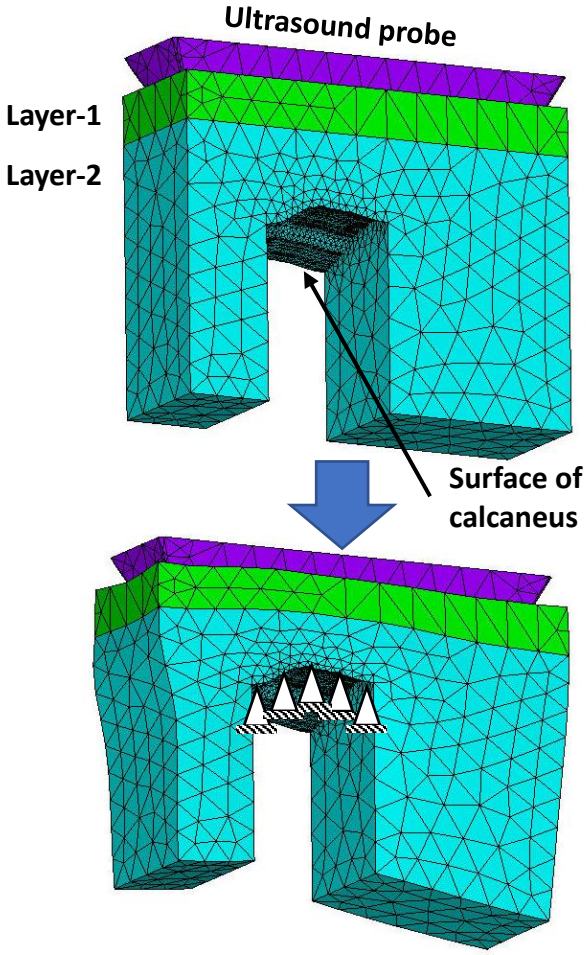

716 Figure 3:
717

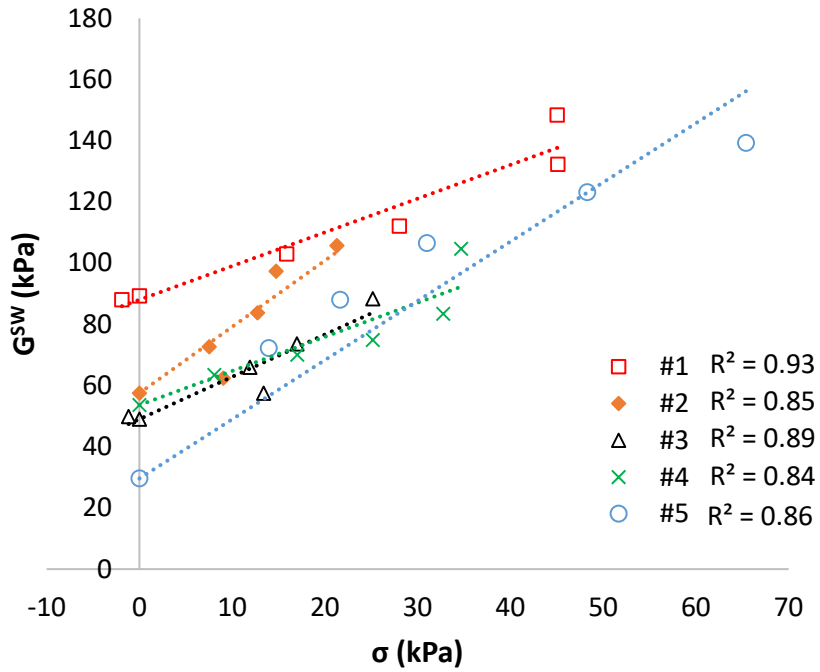

718
719
720
721
722
723
724
725
726
727
728
729
730
731
732
733
734
735
736
737
738
739
740
741
742
743
744
745
746
747
748
749
750

Figure 4:

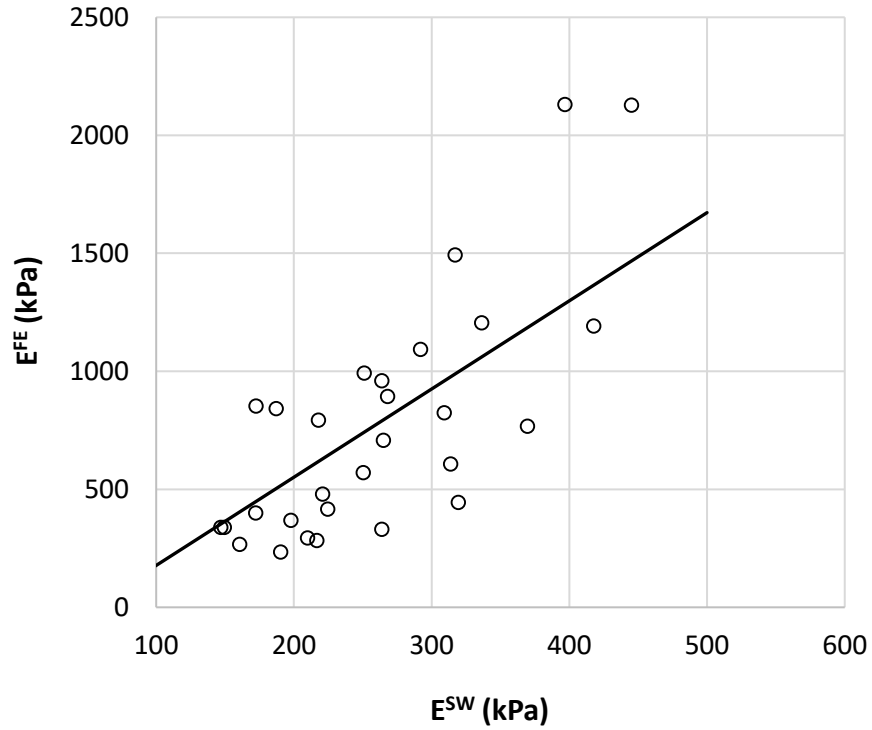

784 Figure 5
785
786
787
788

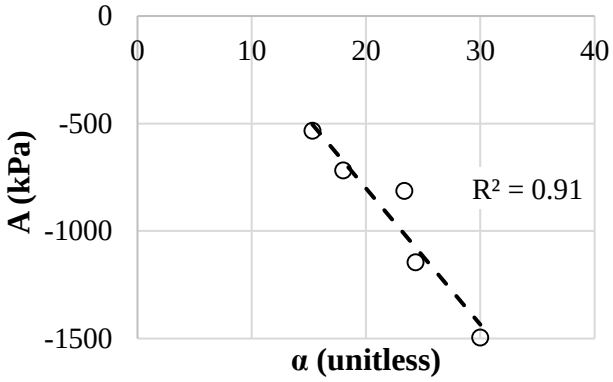

789
790
791
792